Effect of Cyclic Wet-Dry Environment and Vibration Event on Desiccation Crack and Mechanical Characteristics of Polypropylene Fiber-Reinforced Clay

Usama Khalid [a], Zia ur Rehman [b*], Ashfaq Ahmad [c]

[a] National Institute of Transportation (NIT) Risalpur, National University of Sciences and Technology (NUST), Islamabad, 44000, Pakistan. Email: usama.khalid@nit.nust.edu.pk

[b] School of Engineering, College of Science and Engineering, University of Derby, Derby DE22 3AW, United Kingdom. Email: z.rehman1@derby.ac.uk

[c] National Institute of Transportation (NIT) Risalpur, National University of Sciences and Technology (NUST), Islamabad, 44000, Pakistan. Email: aafaq555555@yahoo.com

[*]Corresponding author
Email: z.rehman1@derby.ac.uk; engr.zrehman@gmail.com (Zia ur Rehman)

Abstract: This study investigates the role of polypropylene fibers (PFs) in mitigating the combined effects of wet-dry (W-D) cycles and vibration event (VE), such as earthquakes or machine vibrations, on the desiccation cracking and mechanical behavior of clay through model tests. A comprehensive experimental program was conducted using compacted clayey soil specimens, treated with various PF percentages (0.2%, 0.4%, 0.6%, and 0.8%) and untreated (0%). These specimens were subjected to multiple W-D cycles, with their behavior documented through cinematography. Desiccation cracking and mechanical responses were evaluated after each W-D cycle and subsequent VE. Results indicated that surface cracking, quantified by morphology and crack parameters i.e., crack surface ratio (R_{sc}), total crack length (L_{tc}), and crack line density (D_{cl}), increased with progressive W-D cycles. Higher PF content in soil significantly reduced desiccation cracking across all W-D phases, attributable to the enhanced tensile strength and stress mitigation provided by the fibers. Following VE, surface crack and fragmentation visibility decreased due to the shaking effects, as indicated by reductions in R_{sc} and D_{cl}. However, L_{tc} increased slightly, suggesting either crack persistence or lengthening. Higher PF content resulted in a more substantial reduction in R_{sc} and D_{cl} and a smaller increase in L_{tc} after seismic shaking. W-D cycles led to increased cone index (CI) values, reflecting enhanced compactness due to shrinkage which enhances with PF content showing improved soil resistance to loading. Meanwhile, seismic shaking reduced CI values following W-D cycles, particularly in near-surface layers, PF content mitigates this reduction, demonstrating that PF contributes to a more stable soil matrix. Also, PF content decreased the soil deformation under W-D cycles and subsequent VE.

Keywords: desiccation cracking, mechanical behavior, deformation behavior, wet-dry cycles, vibrations

1. Introduction

Clayey soils, characterized by their hydrophilic mineral composition, are commonly encountered in scenarios that impact ground stability and clay-based building materials. Clay is a fundamental material in building construction due to its widespread availability and versatility, its performance under varying environmental conditions requires further exploration to enhance infrastructure resilience. These minerals exhibit significant volumetric changes in response to moisture fluctuations, leading to pronounced deformations. Such volumetric instability of clayey soils results in extensive damage to civil engineering structures, thereby compromising their integrity and stability [1]. This problem is further intensified when these soils are subjected to complex loadings and climatic conditions [2,3]. Consequently, the design of earthworks involving such soils must carefully consider these adverse effects and implement effective mitigation strategies.

Extensive research has highlighted that wet-dry (W-D) cycles can severely impair critical soil properties such as shear strength, permeability, and infiltration capacity, thereby compromising soil structural integrity [4,5]. One of the most significant issues associated with volumetric changes in clayey soils due to moisture variation from W-D cycles is cracking [6]. Clays are particularly prone to cracking during desiccation because the tensile stress developed within the soil matrix can exceed its inherent tensile strength [7]. The consequences of desiccation cracking extend across various fields, including construction, engineering geology, and agriculture [8]. To address this issue, numerous treatment methods have been proposed, with one common approach being the incorporation of cementing additives or fibers to enhance the tensile strength of the clayey soil matrix and mitigate desiccation cracking [9,10]. However, practical considerations for ground stabilization can be more complex. For example, regions susceptible to moisture variations due to climatic conditions, which induce cyclic W-D

environments, may also experience vibration events (VEs), e.g., earthquake [11]. Additionally, VEs include shaking induced by man-made vibratory sources, e.g., machines, moving vehicles, and railways. VE can further exacerbate cracking and increase deformation in affected soils, necessitating a more comprehensive strategy for mitigating both desiccation cracking and dynamic failures due to VE [3,12]. However, the literature review revealed a significant gap in analyzing soil stabilization of clayey soils, particularly in addressing the mitigation of desiccation cracking under the influence of climatic variations due to W-D cycles and the combined impact of VE.

Fiber reinforcement in clay has been identified in previous studies as an effective strategy for enhancing tensile strength and ductility. The increase in tensile strength helps in mitigating the crack formation by counteracting the tensile stresses induced by W-D cycles within the soil matrix. [13–16]. The fiber reinforcement has been found to have the potential to reduce the average width, total length, and connectivity of soil cracks, thereby improving soil integrity [17,18]. Additionally, the improvement in ductility due to fiber reinforcement enhances the soil's resistance to sudden loading, such as that experienced during earthquakes or vibration events, as demonstrated in past research [16]. Considering this, polypropylene fibers (PFs) are envisaged to play a crucial role in construction, particularly in mitigating desiccation cracking and enhancing soil resistance to dynamic forces [19].

Polypropylene fibers (PFs) are widely recognized for their effectiveness in soil reinforcement due to their cost efficiency, availability, and resistance to environmental conditions [20–23]. Meanwhile, polypropylene waste poses a significant environmental threat, contributing to long-term ecosystem degradation and persisting in the environment for centuries. Recycling polypropylene waste as PFs in the construction industry for soil reinforcement presents a sustainable solution, helping to mitigate plastic waste accumulation, which currently stands at

approximately 260 million tonnes annually and is projected to reach 460 million tonnes by 2030. Previous studies have evaluated PF-reinforced clay under wetting-drying conditions using small-scale thin samples to assess its long-term performance [10,17,24]. These studies have demonstrated the effectiveness of PF in mitigating formation and extent of desiccation cracking. However, past research has primarily focused on crack formation analysis in PF-reinforced clay, with limited emphasis on the crack-influenced strength characteristics of PF-stabilized soils, which is critical from a geotechnical design perspective. Furthermore, the effectiveness of polypropylene fiber-reinforced clay (PFRC) in addressing both desiccation cracking and strength behavior within the complex interplay of W-D cycles and VE in compacted soil has not been investigated. This gap largely stems from the challenges associated with experimentally simulating these combined conditions. Meanwhile, the simultaneous effects of W-D cycling and VE are of significant concern in earthquake-prone regions and areas subject to machine-induced vibrations, particularly where cyclic moisture variations occur due to climate change or seasonal fluctuations. Thus, quantifying the behavior of PF-reinforced soil under these dual environmental and dynamic stressors is crucial, as it provides valuable insights into the resilience of PFRC and informs practitioners about its applicability in sustainable and resilient infrastructure. Although a few previous studies have explored PF-reinforced soil stabilization under cyclic W-D conditions, no research has comprehensively examined the twofold effects of W-D cycling and VE on the desiccation cracking and mechanical behavior of PFRC. This study addresses this gap by evaluating the coupled influence of these environmental and dynamic loading factors, offering new insights into the long-term stability of fiber-reinforced soils under realistic field conditions. The findings contribute to optimizing soil stabilization techniques for infrastructure exposed to both climatic variations and mechanical vibrations.

Considering the foregoing discussion, this study focuses on evaluating the effects of PF under W-D environments, in conjunction with VE, on desiccation cracking and mechanical behavior of clayey soil. This study seeks to address the identified research gap through a comprehensive experimental investigation using a meticulously designed physical model. Large, thick, compacted specimens, prepared with varying percentages of PF, are subjected to W-D cycles and simulated VE to accurately replicate the coupling of W-D environments and VE for naturally compacted soil. Surface crack patterns, strength parameters, and deformations are systematically measured throughout the W-D cycles and following VE. Additionally, Vernier caliper arrangements and Military Engineering Experimental Establishment (MEXE) cone penetrometer (MCP) tests are conducted to assess the impact of desiccation cracks on the strength and deformation of the PFRC. Through a thorough investigation of these factors, this study provides significant insights into the performance of PFRC in the complex interactions between W-D climates and VE, with respect to soil cracking and mechanical behavior.

2. Materials and methods

2.1. Materials

2.1.1. Selected Soil

This study used clayey soil with physical and chemical properties typical of soil undergoing desiccation cracking for stabilization using PF, selected from the Chenab River plain, located in the Punjab province of Pakistan, near Gujranwala. The area's geology is largely defined by alluvial deposits, which are recognized for containing fine-grained soils with a wide range of plasticity [25,26]. The clay's detailed physical properties are listed in Table 1. The grain size distribution curve demonstrate that soil has predominant fraction of fine particles having size less than 0.075 mm (Fig. 1a). According to the Unified Soil Classification System (USCS), the soil is classified as lean clay (CL), based on its grain size distribution and consistency limits.

The soil's composition includes 38.10% clay fraction, 56.60% silt fraction, and 5.30% sand fraction. The liquid limit (w_L) and plasticity index (I_P) were determined to be approximately 44.50% and 20.25, respectively. Moreover, the dominant oxides in the selected clay sample include silicon dioxide (SiO_2) at 55.58%, aluminum oxide (Al_2O_3) at 24.53%, and iron oxide (Fe_2O_3) at 4.25%. These oxides are associated with active clay minerals that often exhibit significant swell-shrink behavior [27]. They play a crucial role in the soil's expansive properties. Their presence influences the soil's interaction with moisture variations and mechanical stresses. The compaction curve was drawn through standard proctor test shows that soil has a maximum dry density (γ_{dmax}) and optimum moisture content (w_{opt}) of 15.85 kN/m^3 and 17.60%, respectively (Fig. 1b). The physical and chemical characteristics of the soil indicate that the selected clayey soil could undergo volume and strength changes under moisture variations, making it suitable for the current study.

2.1.2. Polypropylene fiber (PF)

Polymerized-Olefin PFs were sourced for this study (Fig. 1c). The procured PFs are hydrophobic and chemically inert, ensuring that they do not interact with or absorb soil moisture; thus, their interaction with soil is of a physicomechanical nature [28]. The detailed properties of PF are illustrated in Table 2. PF has a blended length between 5-6 mm with diameter of around 10 µm. PF has a tensile strength of 472 MPa, demonstrating its potential for durability by resisting mechanical degradation. Additionally, its melting point of 162°C and ignition temperature of 593°C indicate thermal stability, while its alkali and acid resistance ensure chemical stability. These properties collectively suggest that PF fibers can effectively resist degradation and maintain their reinforcing function in soils subjected to cyclic moisture variations and loads. The PF content varied from 0.0% to 0.8%, with increments of 0.2% by

weight of soil for each trial, following the approach outlined in the literature on fiber-reinforced clay [29].

2.2. Specimens remolding

After field collection, the natural clay samples underwent a detailed specimen preparation process to ready them for testing. The clayey samples were first dried in an oven at 60°C to remove all moisture. After drying, the clay was pulverized to eliminate any lumps and then passed through a No. 4 sieve to ensure a consistent particle size distribution, which is key for uniform compaction and testing. PFs were then mixed with dry soil and thoroughly blended to ensure uniform distribution before adding water. This dry mixing process prevented fiber clumping and ensured even dispersion throughout the soil. For treated samples, the soil was combined with water and PF at varying concentrations of 0.2%, 0.4%, 0.6%, and 0.8% to ensure an even mixture. The soil was thoroughly mixed with water to achieve a homogeneous consistency. This pre-wetting process is critical for achieving uniform water distribution within the soil, which impacts the compaction and mechanical properties of both treated and untreated soils. The pre-wetted samples were then sealed in plastic covers and left to equilibrate for at least 24 hours, ensuring the moisture was evenly distributed throughout the soil matrix, essential for accurate and reproducible compaction results (Fig. 2 (step 1)).

After equilibration, the specimens were readied for remolding. The pre-wetted soil was subjected to dynamic compaction using a hammer within a custom mold. The compaction process was carefully managed to achieve the required sample thickness of 101.6 mm. This step is crucial, as the level of compaction directly affects the mechanical properties and behavior of the soil under testing conditions. It is noteworthy that the prepared specimens were subjected to VE on the shaking table with imposed boundary conditions that accurately simulated continuous constraints viable for cracking and seismic shaking of soil specimens

[30]. These boundary conditions ensured that the specimens were held securely throughout the shaking process, allowing for precise simulation of VE and reliable measurement of the soil's response. The detailed procedure for specimen remolding is depicted in Fig. 2 (step 1). The prepared specimens were then subjected to W-D cycles and VE, during which various measurements and tests were conducted. A detailed test matrix for this study is presented in Table 3, providing a comprehensive overview of the experimental conditions and parameters.

2.3. Design of mold and shaking table

The dimensions of the mold to prepare the compacted soil specimen of 101.6 mm thickness for W-D Cycles and subsequent testing were 187.96 mm by 187.96 mm by 203.2 mm. Following the W-D cycles, this mold was placed in an outer frame, sized 254 mm by 254 mm by 304.8 mm, which had 12.7 mm springs installed around the edges to function as a damping system representing the boundary conditions for soil specimen that accurately simulated continuous constraints allowing for precise simulation of VE following [31,32], and reliable measurement of the soil behavior, as illustrated in step 4 of Fig. 2 and Fig. 3. The outer frame was then attached to a 1D shaking table capable of simulating VE with uniaxial motion, as also depicted in step 4 of Fig. 2 and Fig. 3. The specifications of the shaking table are detailed in Table 4.

W-D cycles

Two consecutive W-D cycles were conducted on various specimens to assess the impact of climatic variations on crack propagation and mechanical properties. The W-D procedure was based on the methodologies outlined by [33] and [34]. During the wetting phase, each specimen received 250 ml of de-aired water, followed by sealing with plastic wrap for 24 hours to achieve even moisture distribution. After removing the plastic wrap, the specimens were left to air dry in a controlled environment set at 25±5 °C and 35±5% relative humidity. The first drying cycle was considered complete once the specimen's moisture content returned to its initial level (w_0).

Moisture loss was periodically monitored by weighing the specimens. This wetting and drying sequence was repeated for two cycles, with each wetting stage consistently using 250 ml of de-aired water. This methodology offers valuable insights into the behavior of clays subjected to cyclic moisture changes, aiding in the understanding of desiccation crack formation and mechanical responses. The W-D method used for the specimens is depicted in Step 2 of Figure 2.

2.4. Cinematography: Image processing and cracks quantification

The crack propagation was recorded through the cinematography of the specimens. To systematically manage the magnification and size of images for specimen photography, a standardized setup was implemented (Fig. 3c). Images were taken from a constant height, angle, and distance, with light intensity carefully controlled. A white backdrop was used around the specimens to boost contrast and assist with image processing. Photographs were captured from a top view after each W-D, as well as after VE, as shown in Fig. 2 (step 2). The analysis of crack patterns involved using ImageJ software to process these images. The detailed methodology for processing images and quantifying crack patterns is presented in Figs. 2 (step 3) and 4.

The crack analysis included measuring parameters such as crack area (A_c), crack perimeter, and total crack length (L_{tc}) directly from the images. L_{tc} was derived by approximating the distance between intersecting points after the image underwent skeletonization, as demonstrated in Fig. 4. The A_c represents the total area of all cracks on the specimen. Meanwhile, to objectively quantify cracking, the crack surface ratio (R_{sc}), also known as the crack intensity factor (CIF), was calculated as the ratio of the A_c to the total surface area of the soil specimen, indicating the extent of surface cracking. Meanwhile, the crack line density (D_{cl})

was calculated to quantify the degree of surface fragmentation, which is the ratio of the total crack perimeter to the A_c.

2.5. Selection of initial compaction state and vibration events

To determine the density and moisture conditioning of the specimens for evaluating the performance of PF-treated soil, the impact of density was preliminarily assessed for untreated specimens. The initial water content (w_0) was selected on the wet side of the compaction curve of the untreated soil, set at 18% to simulate wet conditions (Figure 1). Subsequently, three initial dry densities (γ_{d0}) were chosen for evaluation, ranging from 13 kN/m^3 to 16 kN/m^3, in increments of 1.5 kN/m^3. It was observed that after the second W-D cycle, a decrease in the γ_{d0} resulted in an increase in R_{sc}, D_{cl}, and L_{tc}, indicating a direct proportionality among desiccation cracking and γ_{d0} (Figs. 5-6). Based on these findings, all soil specimens were prepared with an w_0 of 18% and an γ_{d0} of 14.5 kN/m^3. This selection was made to ensure that the testing matrix was not exhaustive but still incorporated a reasonable high initial cracking condition. Additionally, since an increase in γ_{d0} reduces cracking, a lower density than the γ_{dmax} was selected to assess the performance of PF treatment effectively. The influence of γ_{d0} on desiccation cracking is envisaged to remain directly proportional for PF-treated soil; therefore, it was not included in the primary scope of this study.

Furthermore, to determine the VE in terms of Peak Ground Acceleration (PGA) for evaluating PF-treated soil, the impact of different PGAs on untreated soil was quantified. Three PGA levels, i.e., 0.3g, 0.7g, and 1.16g as shown in Fig. 7, were selected for a duration of 40 seconds to match the seismic history of the region, covering medium to high seismicity and high range of machine-induced vibrations [35–37]. The results indicated that the R_{sc} and D_{cl} decreased while L_{tc} increased with increasing PGA (Fig. 8). Thereby, for testing the PF-treated soil, the shaking table was set to a reasonable worst-case excitation characterized by a PGA level of

0.70g, lasting 40 seconds. Moreover, the impact of PGA is expected to be similar for PF-treated soil, and thus, it was not considered as a variable in the primary scope of the study.

2.6. Mechanical performance tests

The MCP, employed in both field and laboratory settings, was used to measure the specimen's strength characteristics. This device measures the Cone Index (CI), which serves as an indirect indicator of the soil's load-bearing capacity, compaction quality, and strength. It is especially effective for assessing cohesive soils, such as clays. In this study, the MCP testing was conducted after each phase of W-D cycles and VE. The MCP setup for the test included a CI cone, a top rod, and three 150 mm extension rods, as shown in Figure 3d. The penetrometer was inserted into a 101.6 mm thick soil sample to a depth of 76.2 mm, and CI measurements were recorded at 25.4 mm, 50.8 mm, and 76.2 mm depths. Additionally, to further evaluate the treated and untreated soils, deformation was assessed after each W-D cycle and VE. Moreover, the deformation was measured using a Vernier caliper, a precise instrument capable of measuring small dimensional changes with an accuracy of up to 0.02 mm. The calipers were used to measure the initial dimension ($d_{initial}$) and final dimension (d_{final}) of the specimen after exposure to the testing conditions. The deformation (%) was measured as follows:

$$\text{Deformation (\%)} = \left(\frac{d_{initial} - d_{final}}{d_{initial}}\right) \times 100 \quad (1)$$

3. Test results and discussions

3.1. Desiccation cracking

3.6.1. Crack morphology analysis

Fig. 9 illustrates the desiccation cracking morphology of soil, both treated and untreated, across varying stages of W-D cycles and the effects of VE on different soil specimens with PF of 0.2%, 0.4%, 0.6%, and 0.8%, as well as untreated soil (without PF). The impact of W-D cycles

on crack propagation is evident in all specimens, with cracks becoming more prominent as the cycles progress. The cracking becomes visible on the surface after the first drying cycle. This behavior can be attributed to the development of desiccation cracks, primarily driven by the increasing suction or tensile stresses occurring on the specimen surface during the drying process. When tensile stress exceeds the tensile strength of the soil, desiccation cracks initiate on the specimen surface, as observed during the first drying cycle [38]. As the W-D cycles repeat for the second time, the cracks progressively widen and extend after the drying cycle [39]. Furthermore, the application of VE after the second drying cycle demonstrates a reduction in surface crack visibility, as shaking closes the cracks, thereby diminishing their surface appearance.

Fig. 9 also demonstrates that as the percentage of PF increases, the occurrence of desiccation cracking decreases compared to soils with lower PF percentages and untreated specimens. The addition of fibers proves effective in reducing the extent of desiccation cracks and enhancing the soil's resistance to cracking. This improved resistance can be attributed to the increase in tensile strength imparted by the fibers. Incorporating small amounts of PF into the soil matrix strengthens the bond and friction between the fibers and soil particles, thereby restricting the relative movement of the fibers within the matrix [17]. Consequently, the fibers can bear a portion of the tensile stress that develops during drying, thereby reducing the initiation of cracks. These fibers also help to distribute tensile stresses more uniformly throughout the soil matrix, thus lowering the probability of crack formation and propagation. This finding is consistent with previous research studies [17,29], which have demonstrated that fiber reinforcement enhances the mechanical properties of soil, including tensile strength and resistance to desiccation cracking. Also, an increase in PF content enhances the effectiveness of crack reduction following VE after W-D cycles. This also means that the VE does not diminish the crack mitigation performance of the PF in a W-D environment. The analysis

suggests that increasing the PF content in clayey soils is an effective strategy for mitigating desiccation cracking, thereby improving the durability and stability of soil structures subjected to adverse climatic conditions favorable to causing cracking.

The underlying mechanism governing desiccation crack formation and mitigation in PF-reinforced soil observed in the crack morphology analysis involves an interaction between tensile stress development due to W-D cycles, fiber reinforcement, and VE effects. During W-D cycles, water loss increases matric suction, generating tensile stresses that, when exceeding soil tensile strength, lead to crack initiation and propagation [39]. The incorporation of PF gradually enhances soil tensile strength by improving interfacial bonding and friction, thereby restricting crack formation and propagation. Additionally, VE excitation following W-D cycles aids in closing surface cracks by redistributing stresses and soil mass, thereby reducing their surface visibility.

3.6.2. Crack parameter analysis

To quantify desiccation cracking, R_{sc}, D_{cl}, and L_{tc} were analyzed in Figs. 10-12 for all specimens subjected to different W-D cycles and subsequent VE. It was observed that R_{sc}, which directly indicates the extent of cracking, becomes prominent at the completion of the drying cycle, with its magnitude increasing as the W-D cycles progresses (Fig. 10). Conversely, R_{sc} slightly decreases from the drying phase upon the application of VE, suggesting a reduction in surface crack visibility [8]. A similar response was noted for D_{cl}, highlighting the role of W-D cycles and their interaction with VE on the degree of surface fragmentation of cracked soil samples (Fig. 11). Interestingly, the impact of W-D cycles on L_{tc} was consistent with the trends observed for R_{sc}, D_{cl}, across all specimens (Fig. 12). However, after the application of VE following the second drying cycle, L_{tc} displayed a reverse trend, slightly increasing with the application of shaking. This indicates that, although VE reduces apparent surface cracking and the degree of surface fragmentation, the cracks retain or enhance their length [40]. This

counterintuitive result can be attributed to stress redistribution and structural realignment under vibrational stressor. Under VE, the compression or compaction of clay may narrow and reduce the visible area of surface cracks. However, this process can also induce internal stresses that potentially lengthen surface cracks. Despite the decreased visibility of surface cracks, their lengthening can still contribute to the overall deformation of the clay.

The addition of PF was observed to reduce R_{sc}, D_{cl}, and L_{tc} during all W-D cycle phases, indicating that PF contributes essential tensile strength that is lost due to desiccation cracking. This effect becomes more pronounced with increased PF content (Figs. 10-12). Additionally, PF aids in managing the stress redistribution impact of VE on cracks induced by W-D cycles, with R_{sc}, D_{cl}, and L_{tc} consistently showing significantly lower values in treated samples compared to untreated ones with increase in PF content. This means that PF not only further reduces surface crack visibility but also diminishes the impact of VE on L_{tc} by mitigating stress redistribution and minimizing the potential for surface crack lengthening that could cause ground deformation [41].

Overall, mechanistically, as W-D cycles progress, the extent of surface cracking in terms of R_{sc}, D_{cl}, and L_{tc} increase due to repeated shrinkage and stress buildup. On the other hand, VE reduces surface crack visibility and fragmentation by compacting the soil, but it also redistributes stresses, potentially elongating cracks internally as depicted by increase in L_{tc}. The addition of PF mitigates these effects by enhancing tensile strength, restricting crack initiation and propagation, and counteracting VE-induced stress redistribution. Higher PF content leads to a significant reduction in R_{sc}, D_{cl}, and L_{tc}, effectively minimizing desiccation cracking and preventing excessive deformation. These findings underscore the effectiveness of PF in mitigating the combined effects of cyclic W-D conditions and VE, thereby enhancing the resilience of infrastructure constructed on such soils.

3.2. Mechanical characteristics

3.2.1. Strength behavior

Fig. 13 illustrates the effect of different phases of W-D cycles and subsequent VE on the CI values of untreated and treated soils at depths of 25.4 mm, 50.8 mm, and 76.2 mm. Across all specimens and depths, CI increases as the W-D cycles progress. A similar trend is observed during the subsequent wetting and drying phases, though the CI values are lower in the wetting phase due to elevated moisture content. The increase in CI with W-D cycles can be attributed to the repeated shrinkage of soil particles during drying, resulting in pore space reduction, densification, and hardening of the soil matrix. Each W-D cycle enhances soil compaction, thereby increasing its resistance to cone penetration, as reflected in CI values [25]. Additionally, VE after the second drying cycle reduces CI across all specimens and depths, highlighting the effect of VE, which redistributes stresses and weakens the soil's resistance to cone penetration. This reduction can be attributed to the loosening of the soil structure caused by VE. Meanwhile, the percentage decrease in CI before and after VE (ΔCI_{VE}) is higher at shallower depths and lower at greater depths, suggesting the influence of overburden and desiccation cracking in the upper layers, which cause greater disruption of the soil structure near the surface (Fig. 14).

The presence of PF was observed to significantly impact CI in all phases of the W-D cycles across the depths (Fig. 13). Untreated soil exhibits lower CI values compared to PF-treated specimens, and soils with higher PF content show larger CI values than those with lower PF percentages in all W-D phases across all depth intervals. Furthermore, the increase in CI with an increase in W-D cycles is more pronounced in soil specimens with higher PF content. This enhancement is attributed to the fibers' ability to reinforce the soil matrix, providing additional tensile strength and resistance to cracking. The fibers bind the soil particles together, thereby

376 improving the structural integrity of the soil. Despite the reduction in CI due to VE, PF-treated
377 soils maintain higher CI values than untreated soils, indicating that fiber reinforcement
378 provides resilience against seismic-induced weakening which increases with the increase in PF
379 content. This resilience is likely due to the fibers preserving soil integrity under dynamic
380 loading, thereby mitigating the structural degradation typically caused by VE [41].
381 Additionally, PF content reduces ΔCI_{VE} and minimizes the difference between upper and lower
382 layers, as higher PF content creates a more homogeneous soil matrix less prone to disruption
383 by stress redistribution due to VE (Fig. 14). These results underscore the interplay between W-
384 D cycles and VE on the mechanical behavior of the PFRC.

385 The underlying mechanism governing the variation in strength characteristics in terms of CI in
386 PF-reinforced soil under W-D cycles and VE is summarized to be influenced by soil
387 densification, structural integrity, and stress redistribution. As W-D cycles progress, repeated
388 shrinkage and moisture fluctuations lead to soil compaction, reducing pore space and hardening
389 the soil matrix, which increases CI. However, VE disrupts this densified structure by
390 redistributing stresses and loosening the soil, causing a reduction in CI, particularly in the upper
391 layers where desiccation cracking is more pronounced. PF content enhances soil tensile
392 strength and structural integrity by binding soil particles together, leading to higher CI values
393 across all W-D phases and depths compared to untreated soil. Despite VE-induced loosening,
394 PF-treated soils retain greater resistance to penetration due to their reinforced matrix, reducing
395 the ΔCI_{SE} and creating a more uniform soil structure. The higher the PF content, the more

effective the mitigation of VE-induced weakening, highlighting the role of fiber reinforcement in improving soil resilience under both cyclic environmental and dynamic loading conditions.

3.2.2. Deformation behavior

Fig. 15 illustrates the deformation behavior of PF-treated and untreated soils, considering the combined effects of W-D cycles and VE. The soil exhibits positive deformation (swelling) during the wetting phase and negative deformation (shrinkage) during the drying phase. Overall, deformation (i.e., swell-shrinkage %) decreases in the second W-D cycle compared to the first, indicating the progressive stabilization of the soil matrix due to repeated moisture fluctuations for all specimens. As the soil undergoes successive W-D cycles, particles become more densified and reoriented, leading to a more stable structure with reduced volumetric changes [42]. This observation is consistent with the enhancement in strength characteristics associated with increasing W-D cycles. Additionally, VE affects deformation behavior, with negative deformation (shrinkage) increasing after VE. This response to seismic loading, characterized by heightened shrinkage, is attributed to the rearrangement of soil particles under VE.

PF content was found to significantly influence the overall deformation (swell-shrinkage%) potential. Increased PF content notably reduces positive deformation during the wetting phase, thereby maintaining lower overall deformation throughout W-D cycles. This relationship indicates that higher PF content provides enhanced reinforcement. PF improves soil stability by increasing tensile strength and serving as a binding agent that interlocks soil particles. This interlocking mechanism ensures more uniform stress distribution across the soil matrix, effectively mitigating deformation and improving overall soil stability. Additionally, the presence of PF significantly reduces post-SE deformation due to the reinforcing effect of fibers

within the soil matrix, which limits stress redistribution and the impact of particle rearrangement, thus controlling the extent of deformation.

Thus, the underlying mechanism governing deformation behavior in PF-treated and untreated soils under W-D cycles and VE is driven by soil densification, particle rearrangement, and fiber reinforcement. During wetting, soil swells due to moisture absorption, while drying induces shrinkage due to moisture loss, with overall deformation decreasing in the second W-D cycle as the soil matrix stabilizes through progressive compaction and particle reorientation. VE further amplifies shrinkage by inducing particle rearrangement and stress redistribution. The addition of PF enhances soil stability by increasing tensile strength and interlocking soil particles, reducing excessive swelling during wetting and mitigating shrinkage after VE. Higher PF content improves stress distribution, limits volumetric changes, and minimizes deformation caused by VE, demonstrating the role of PF reinforcement in maintaining soil integrity under cyclic environmental and dynamic stressors.

4. Conclusions

This comprehensive investigation into the coupled impact of W-D cycles and VE, for untreated and PF-treated soils on the desiccation cracking, strength, and deformation characteristics has yielded valuable insights as discussed below:

- Desiccation cracking intensifies with W-D cycles, especially during drying, but increasing PF content significantly reduces cracking by enhancing the soil's tensile strength. VE reduces the visibility of surface cracks, with higher PF content providing greater crack mitigation.
- The R_{sc}, L_{tc}, and D_{cl} increase with W-D cycles, indicating more cracking, but these parameters are significantly reduced with higher PF content, demonstrating PF's effectiveness in mitigating cracking and surface fragmentation. VE reduces R_{sc} and D_{cl},

but L_{tc} slightly increases indicating redistribution of stresses, potentially elongating cracks internally; however, PF reduces this increase, especially at higher PF levels.

- The CI values rise with W-D cycles due to soil densification from shrinkage, but decrease after VE, particularly in the surface layers where desiccation cracking is more pronounced. PF incorporation enhances soil resistance, reducing the impact of VE on CI, and helps maintain a more uniform, stable soil matrix.
- W-D cycles lead to an increase in deformation, with PF significantly reducing overall deformation throughout the cycles. VE after W-D cycles causes additional shrinkage, but the effect is mitigated by higher PF content, highlighting PF's role in stabilizing soil deformation under combined W-D and vibrational conditions.

This study highlights the effectiveness of PF reinforcement in improving the mechanical properties and crack resistance of clayey soils under cyclic W-D conditions and seismic activity for a specific worst-case compaction state and VE; future studies could focus on other types of fibers and impact of compaction state and PGA on fiber reinforced soils under coupling W-D and VE conditions.

References

[1] F. Ghalamzan, J. De Rosa, A. Gajo, C. Di Maio, Swelling and swelling pressure of a clayey soil: Experimental data, model simulations and effects on slope stability, Eng. Geol. 297 (2022) 106512. https://doi.org/10.1016/J.ENGGEO.2021.106512.

[2] N. Ijaz, W. Ye, Z. ur Rehman, F. Dai, Z. Ijaz, Numerical study on stability of lignosulphonate-based stabilized surficial layer of unsaturated expansive soil slope considering hydro-mechanical effect, Transp. Geotech. 32 (2022) 100697.

[3] Z. Liu, J. Xue, The deformation characteristics of a kaolin clay under intermittent cyclic loadings, Soil Dyn. Earthq. Eng. 153 (2022) 107112. https://doi.org/10.1016/J.SOILDYN.2021.107112.

[4] C.S. Tang, Q. Cheng, T. Leng, B. Shi, H. Zeng, H.I. Inyang, Effects of wetting-drying cycles and desiccation cracks on mechanical behavior of an unsaturated soil, CATENA. 194 (2020) 104721. https://doi.org/10.1016/J.CATENA.2020.104721.

[5] S.G. Goh, H. Rahardjo, E.C. Leong, Shear Strength of Unsaturated Soils under Multiple

Drying-Wetting Cycles, J. Geotech. Geoenvironmental Eng. 140 (2014) 06013001. https://doi.org/10.1061/(ASCE)GT.1943-5606.0001032/ASSET/6EA3B21A-0280-408B-AD44-138963DA083F/ASSETS/IMAGES/LARGE/FIGURE6.JPG.

[6] K. Shafqat, U. Khalid, Z. ur Rehman, Coupling effect of cyclic wet-dry environment and compaction state on desiccation cracking and mechanical behavior of low and high plastic clays, Bull. Eng. Geol. Environ. 84 (2025) 1–26. https://doi.org/10.1007/S10064-024-04049-2/FIGURES/30.

[7] C.S. Tang, Q. Cheng, L. Lin, B.G. Tian, H. Zeng, B. Shi, Study on the dynamic mechanism of soil desiccation cracking by surface strain/displacement analysis, Comput. Geotech. 152 (2022) 104998. https://doi.org/10.1016/J.COMPGEO.2022.104998.

[8] C.S. Tang, C. Zhu, Q. Cheng, H. Zeng, J.J. Xu, B.G. Tian, B. Shi, Desiccation cracking of soils: A review of investigation approaches, underlying mechanisms, and influencing factors, Earth-Science Rev. 216 (2021) 103586. https://doi.org/10.1016/J.EARSCIREV.2021.103586.

[9] Y. Gui, W.Y. Wong, C. Gallage, Effectiveness and Sensitivity of Fiber Inclusion on Desiccation Cracking Behavior of Reinforced Clayey Soil, Int. J. Geomech. 22 (2022) 06021040. https://doi.org/10.1061/(ASCE)GM.1943-5622.0002278/ASSET/61D75665-31D5-480A-8BE1-24326B52A035/ASSETS/IMAGES/LARGE/FIGURE18.JPG.

[10] U. Chaduvula, B.V.S. Viswanadham, J. Kodikara, A study on desiccation cracking behavior of polyester fiber-reinforced expansive clay, Appl. Clay Sci. 142 (2017) 163–172. https://doi.org/10.1016/J.CLAY.2017.02.008.

[11] F. Alshawmar, M. Fall, Investigation of drying and wetting effects on response of highly densified tailings to cyclic loadings: Shaking table test results, Soil Dyn. Earthq. Eng. 166 (2023) 107769. https://doi.org/10.1016/J.SOILDYN.2023.107769.

[12] J.M. Mayoral, E. Castañon, N. Sarmiento, Seismic response of high plasticity clays during extreme events, Soil Dyn. Earthq. Eng. 77 (2015) 203–207. https://doi.org/10.1016/J.SOILDYN.2015.05.013.

[13] I. Ullah, U. Khalid, Z. ur Rehman, M.M. Shah, I. Khan, N. Ijaz, Integrated recycling of geopolymerized quarry dust and bagasse ash with facemasks for the balanced amelioration of the fat clay: a multi-waste solution, Environ. Earth Sci. 82 (2023). https://doi.org/10.1007/S12665-023-11219-0.

[14] F. Hojjati, A. Sarkar, Mechanical properties of soil reinforced with polypropylene fibre, Proc. Inst. Civ. Eng. Constr. Mater. 175 (2022) 72–81. https://doi.org/10.1680/JCOMA.18.00057/ASSET/IMAGES/SMALL/JCOMA.18.00057-F9.GIF.

[15] Z. ur Rehman, U. Khalid, Optimization of COVID-19 face mask waste fibers and silica fume as a balanced mechanical ameliorator of fat clay using response surface methodology, Environ. Sci. Pollut. Res. 29 (2022) 17001–17016. https://doi.org/10.1007/S11356-021-16912-W/FIGURES/7.

[16] Y. Sun, J. Shi, Z. Liu, C. Liu, Y. Zhang, The failure modes of flexible fibers in reinforced soil with different dry densities, Constr. Build. Mater. 449 (2024) 138386. https://doi.org/10.1016/J.CONBUILDMAT.2024.138386.

[17] C.S. Tang, B. Shi, Y.J. Cui, C. Liu, K. Gu, Desiccation cracking behavior of polypropylene fiber-reinforced clayey soil, Can. Geotech. J. 49 (2012) 1088–1101. https://doi.org/10.1139/T2012-067.

[18] D.L. Wang, C.S. Tang, X.H. Pan, B. Liu, B. Shi, Coupling effect of fiber reinforcement and MICP stabilization on the tensile behavior of calcareous sand, Eng. Geol. 317 (2023) 107090. https://doi.org/10.1016/J.ENGGEO.2023.107090.

[19] T. Sengul, N. Akray, Y. Vitosoglu, Investigating the effects of stabilization carried out using fly ash and polypropylene fiber on the properties of highway clay soils, Constr. Build. Mater. 400 (2023) 132590. https://doi.org/10.1016/J.CONBUILDMAT.2023.132590.

[20] N. Liang, S. Geng, J. Mao, X. Liu, X. Zhou, Investigation on cracking resistance mechanism of basalt-polypropylene fiber reinforced concrete based on SEM test, Constr. Build. Mater. 411 (2024) 134102. https://doi.org/10.1016/J.CONBUILDMAT.2023.134102.

[21] M.R. Abdi, H. Mirzaeifar, Effects of discrete short polypropylene fibers on behavior of artificially cemented kaolinite, Int. J. Civ. Eng. 14 (2016) 253–262. https://doi.org/10.1007/s40999-016-0022-5.

[22] K. Roshan, A.J. Choobbasti, S.S. Kutanaei, A. Fakhrabadi, The effect of adding polypropylene fibers on the freeze-thaw cycle durability of lignosulfonate stabilised clayey sand, Cold Reg. Sci. Technol. 193 (2022) 103418. https://doi.org/10.1016/J.COLDREGIONS.2021.103418.

[23] A. Boz, A. Sezer, Influence of fiber type and content on freeze-thaw resistance of fiber reinforced lime stabilized clay, Cold Reg. Sci. Technol. 151 (2018) 359–366. https://doi.org/10.1016/J.COLDREGIONS.2018.03.026.

[24] H.R. Akbari, H. Sharafi, A.R. Goodarzi, Effect of polypropylene fiber and nano-zeolite on stabilized soft soil under wet-dry cycles, Geotext. Geomembranes. 49 (2021) 1470–1482. https://doi.org/10.1016/J.GEOTEXMEM.2021.06.001.

[25] U. Khalid, Z. ur Rehman, H. Mujtaba, K. Farooq, 3D response surface modeling based in-situ assessment of physico-mechanical characteristics of alluvial soils using dynamic cone penetrometer, Transp. Geotech. 36 (2022) 100781. https://doi.org/10.1016/J.TRGEO.2022.100781.

[26] M.M. Shah, H.M. Shahzad, U. Khalid, K. Farooq, Z. ur Rehman, Experimental Study on Sustainable Utilization of CKD for Improvement of Collapsible Soil, Arab. J. Sci. Eng. 48 (2023) 5667–5682. https://doi.org/10.1007/S13369-022-07565-Z/FIGURES/19.

[27] A. Smaida, B. Mekerta, M.K. Gueddouda, Physico-mechanical stabilization of a high swelling clay, Constr. Build. Mater. 289 (2021) 123197. https://doi.org/10.1016/J.CONBUILDMAT.2021.123197.

[28] H. Wang, W. Ni, K. Yuan, Mechanical properties, microstructural evolution, and environmental impacts of recycled polypropylene fiber stabilized loess, Constr. Build. Mater. 400 (2023) 132850. https://doi.org/10.1016/J.CONBUILDMAT.2023.132850.

[29] Z. ur Rehman, U. Khalid, Reuse of COVID-19 face mask for the amelioration of mechanical properties of fat clay: A novel solution to an emerging waste problem, Sci. Total Environ. 794 (2021) 148746. https://doi.org/10.1016/J.SCITOTENV.2021.148746.

[30] M.R. Lakshmikantha, P.C. Prat, A. Ledesma, Boundary Effects in the Desiccation of Soil Layers with Controlled Environmental Conditions, Geotech. Test. J. 41 (2018) 675–697. https://doi.org/10.1520/GTJ20170018.

[31] M. Ilankatharan, B. Kutter, Modeling input motion boundary conditions for simulations of geotechnical shaking table tests, Earthq. Spectra. 26 (2010) 349–369. https://doi.org/10.1193/1.3383214/ASSET/IMAGES/LARGE/10.1193_1.3383214-FIG16.JPEG.

[32] H. Kim, D. Kim, Y. Lee, H. Kim, Effect of Soil Box Boundary Conditions on Dynamic Behavior of Model Soil in 1 g Shaking Table Test, Appl. Sci. 2020, Vol. 10, Page 4642. 10 (2020) 4642. https://doi.org/10.3390/APP10134642.

[33] H. Krisdani, H. Rahardjo, E.C. Leong, Effects of different drying rates on shrinkage characteristics of a residual soil and soil mixtures, Eng. Geol. 102 (2008) 31–37. https://doi.org/10.1016/J.ENGGEO.2008.07.003.

[34] B.G. Tian, Q. Cheng, C.S. Tang, H. Zeng, J. jian Xu, B. Shi, Effects of compaction state on desiccation cracking behaviour of a clayey soil subjected to wetting-drying cycles, Eng. Geol. 302 (2022) 106650. https://doi.org/10.1016/J.ENGGEO.2022.106650.

[35] K. Mahmood, B. Zamin, S. Iqbal, Zia-Ur-Rehman, S. Afzal, M. Safdar, Q. Iqbal, A. Ali, Local site effect on seismic hazard of the relocated new Balakot town, Soil Dyn. Earthq. Eng. 162 (2022). https://doi.org/10.1016/j.soildyn.2022.107451.

[36] K. Mahmood, Z. ur R. Rehman, K. Farooq, S.A. Memon, One dimensional equivalent linear ground response analysis — A case study of collapsed Margalla Tower in Islamabad during 2005 Muzaffarabad Earthquake, J. Appl. Geophys. 130 (2016) 110–117. https://doi.org/10.1016/J.JAPPGEO.2016.04.015.

[37] U. Abid, A. Haider, B. Alshameri, Z. ur Rehman, A.J. Khan, N. Mahmood, S. Hassan, Determination of ground motion parameters of urban centers of Balochistan province, Soil Dyn. Earthq. Eng. 175 (2023) 108221. https://doi.org/10.1016/J.SOILDYN.2023.108221.

[38] H. Peron, T. Hueckel, L. Laloui, L.B. Hu, Fundamentals of desiccation cracking of fine-grained soils: Experimental characterisation and mechanisms identification, Can. Geotech. J. 46 (2009) 1177–1201. https://doi.org/10.1139/T09-054/ASSET/IMAGES/T09-054IE8H.GIF.

[39] S. Bordoloi, R. Hussain, V.K. Gadi, H. Bora, L. Sahoo, R. Karangat, A. Garg, S. Sreedeep, Monitoring soil cracking and plant parameters for a mixed grass species, Geotech. Lett. 8 (2018) 49–55. https://doi.org/10.1680/JGELE.17.00145.

595 [40] R.N. Tollenaar, L.A. van Paassen, C. Jommi, Observations on the desiccation and
596 cracking of clay layers, Eng. Geol. 230 (2017) 23–31.
597 https://doi.org/10.1016/J.ENGGEO.2017.08.022.

598 [41] H. Trabelsi, E. Romero, M. Jamei, Tensile strength during drying of remoulded and
599 compacted clay: The role of fabric and water retention, Appl. Clay Sci. 162 (2018) 57–
600 68. https://doi.org/10.1016/J.CLAY.2018.05.032.

601 [42] Q. Cheng, C.S. Tang, Z. guo Chen, M.R. El-Maarry, H. Zeng, B. Shi, Tensile behavior
602 of clayey soils during desiccation cracking process, Eng. Geol. 279 (2020) 105909.
603 https://doi.org/10.1016/J.ENGGEO.2020.105909.

604 **Nomenclatures**

A_c	Crack area
CI	Cone index
D_{cl}	Crack line density
ΔCI_{VE}	Percentage decrease in CI value after VE
I_P	Plasticity index
L_{tc}	Total crack length
PF	Polypropylene fibers
MCP	MEXE cone penetrometer
PFRC	PF reinforced clay
PGA	Peak ground acceleration
R_{sc}	Crack surface ratio
VE	Vibration event
USCS	Unified soil classification system
W-D	Wetting drying
w	Water content
w_L	Liquid limit
w_0	Initial water content
w_{opt}	Optimum water content
γ_{d0}	Initial dry unit weight

605

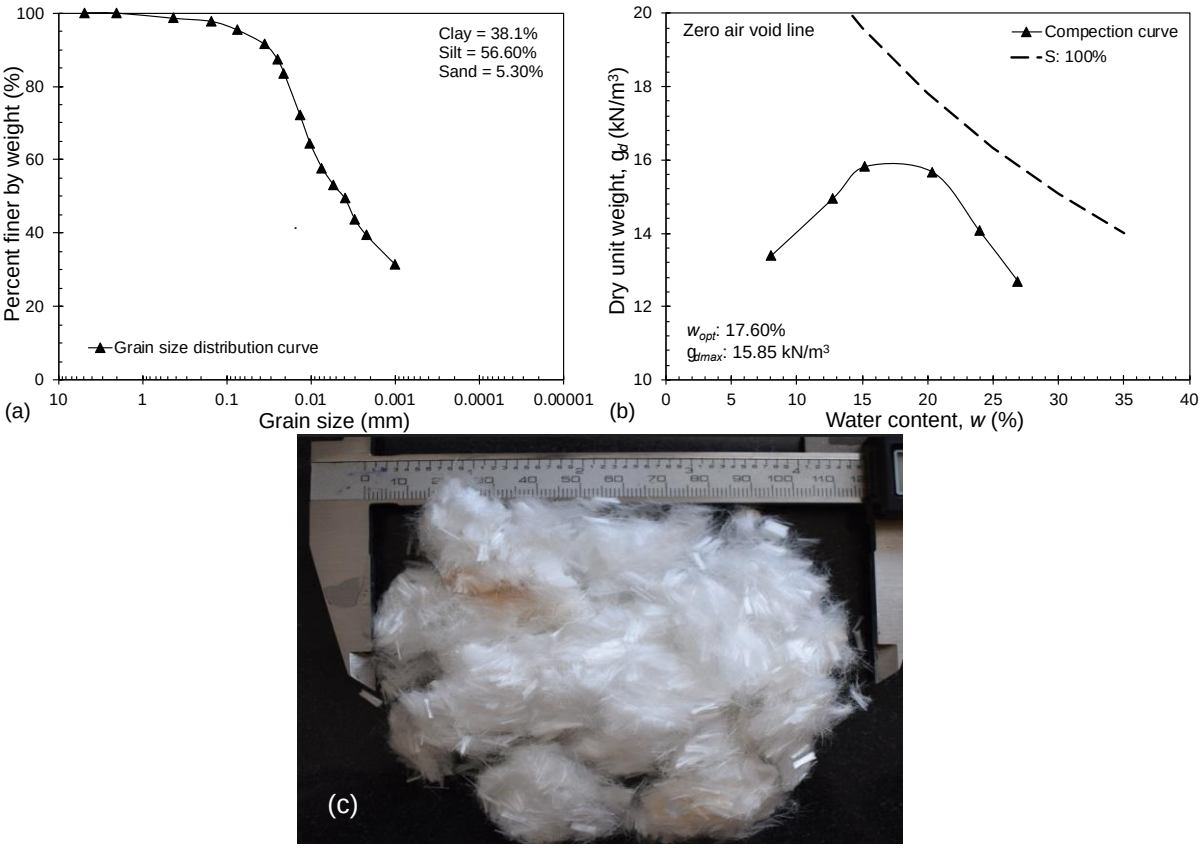

Fig. 1 Selected material characteristics (a) grain size distribution curve; (b) compaction curve determined by standard compaction test; (c) fiber demonstration

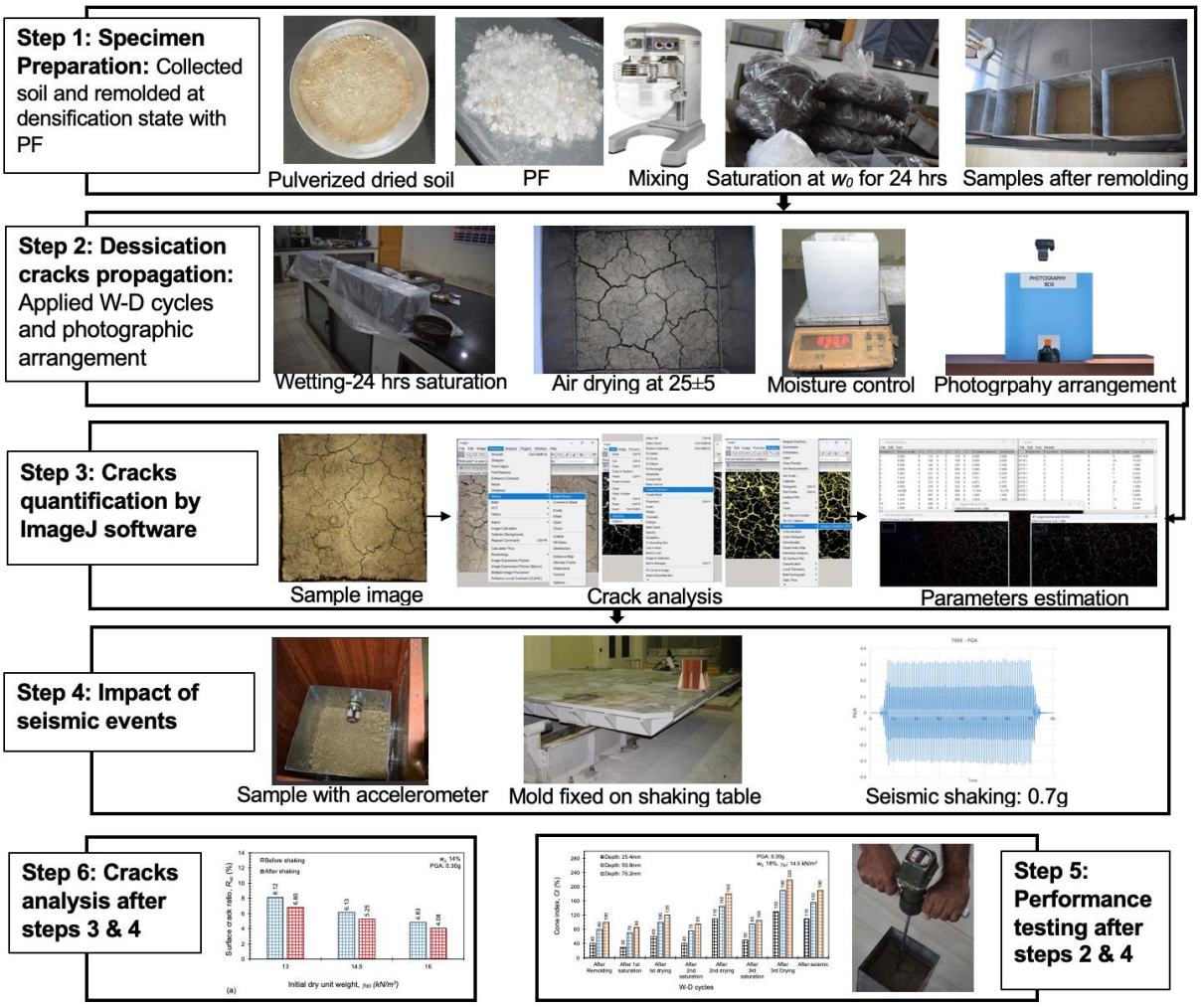

Fig. 2 Methodology of the current study

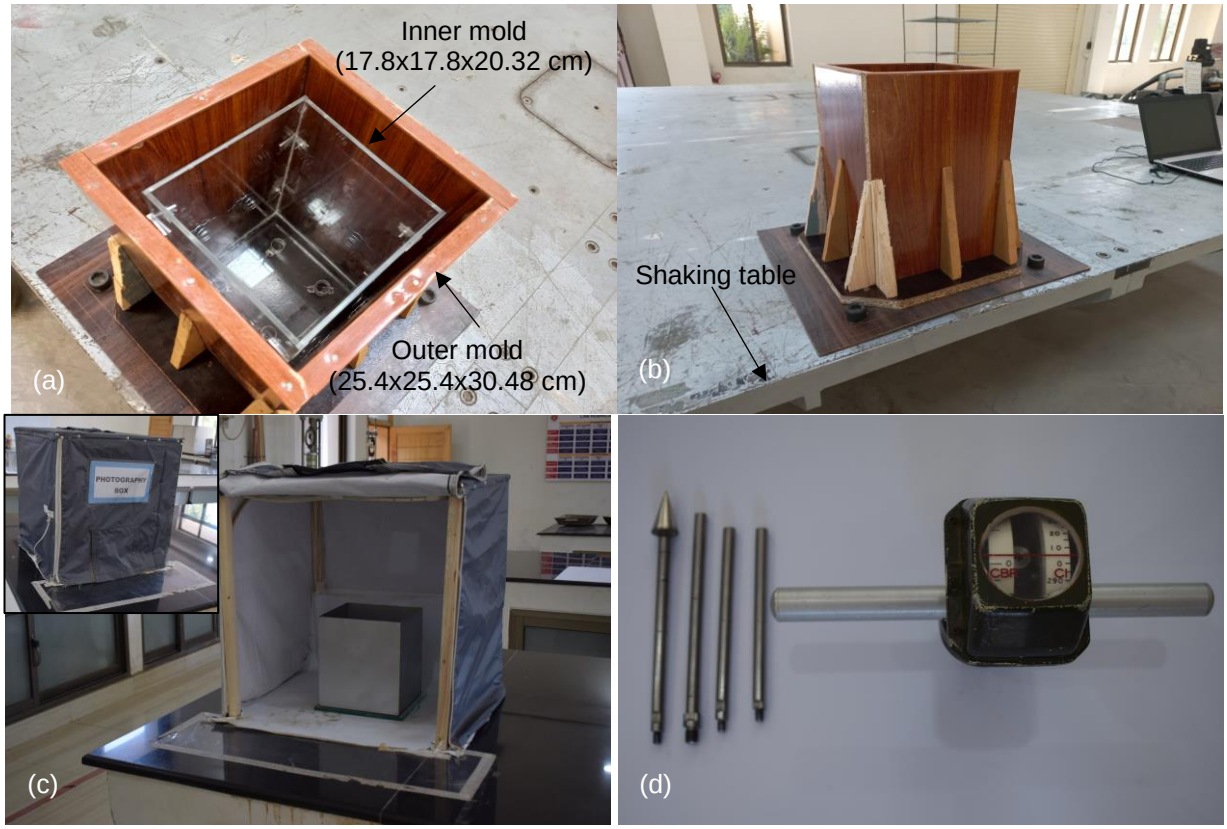

Fig. 3 Experimental arrangement for the current study (a) damping system; (b) damping system installed on shaking table; (c) photography set up (d) MEXE cone penetrometer

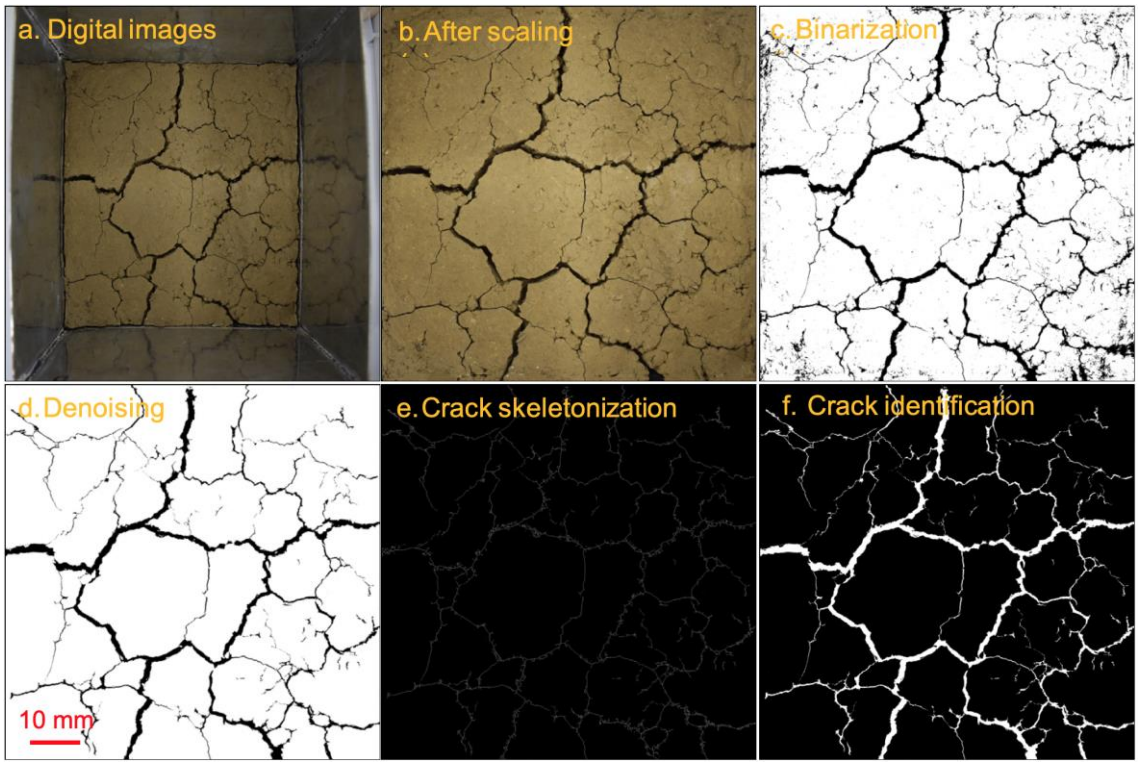

Fig. 4 Steps of crack image processing

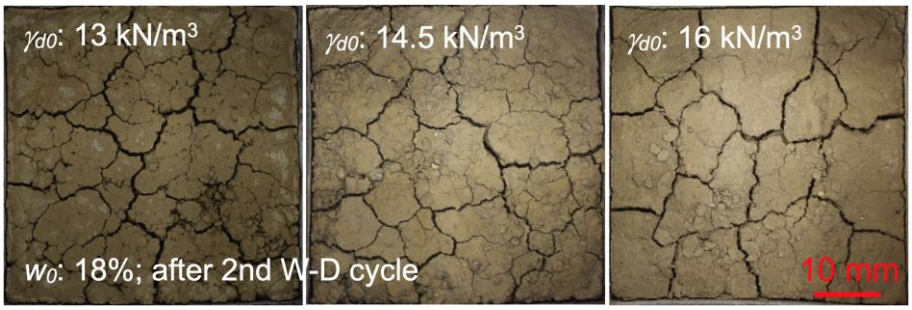

Fig. 5 Effect of densification on cracks morphology of untreated samples

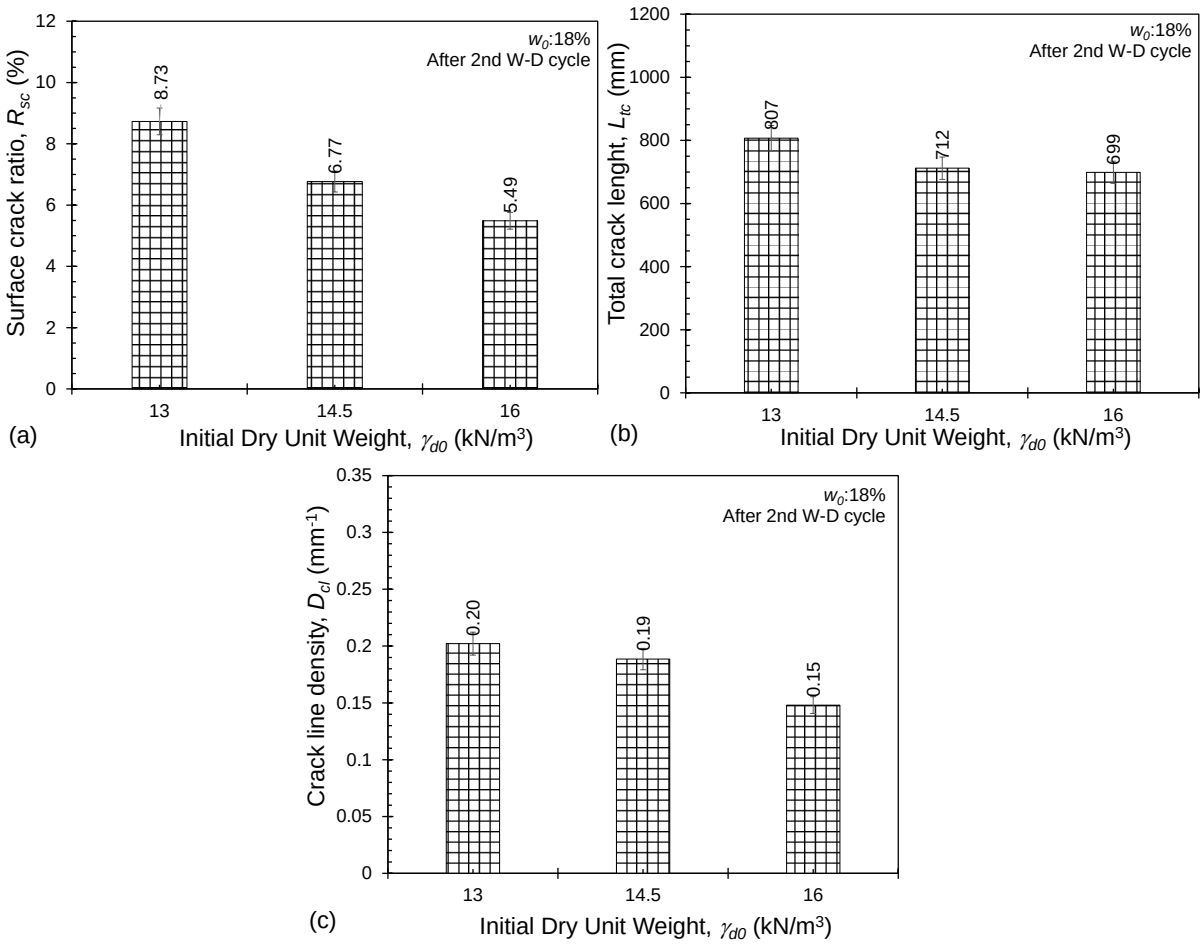

Fig. 6 Effect of densification on (a) R_{sc}; (b) L_{tc}; (c) D_{cl} of untreated samples

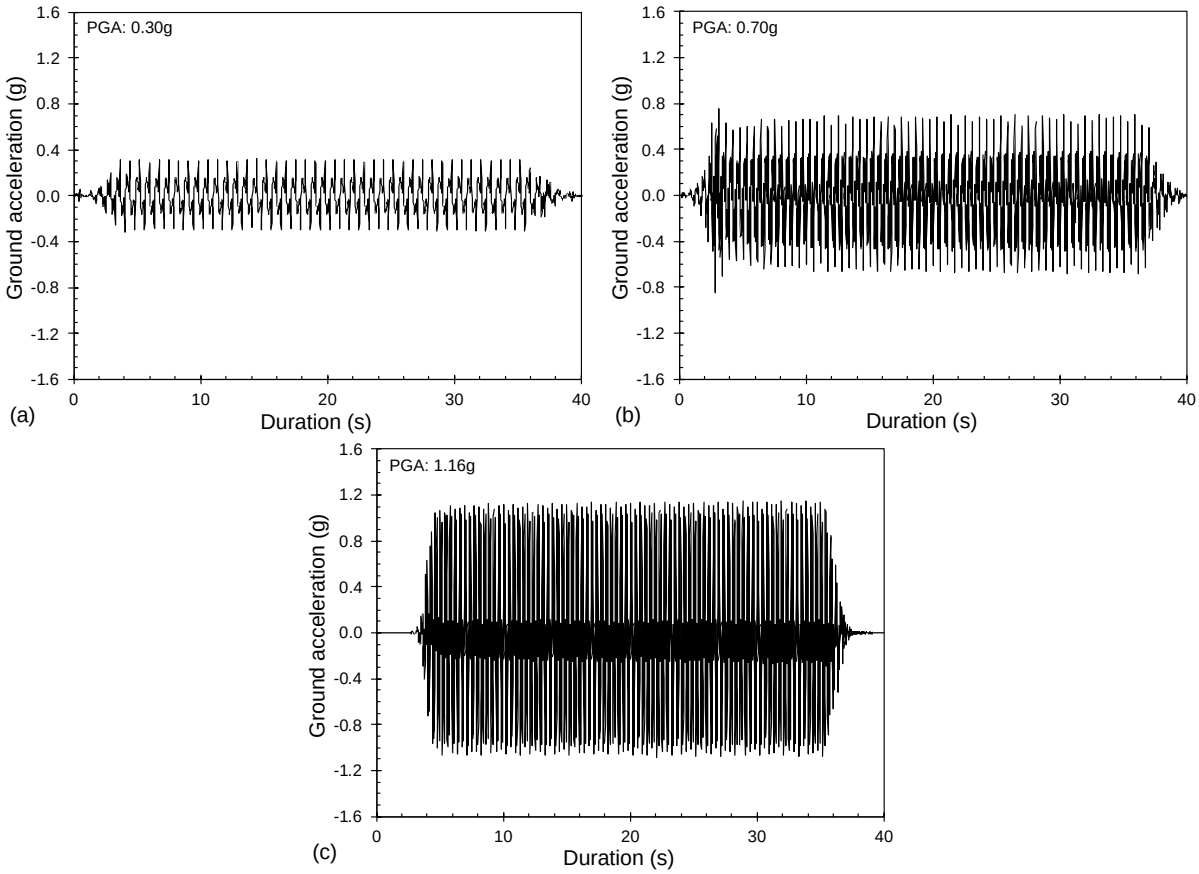

Fig. 7 Shaking spectra of selected VE (a) PGA: 0.30g; (b) PGA: 0.70g; (s) PGA: 1.16g, applied for about 40 s

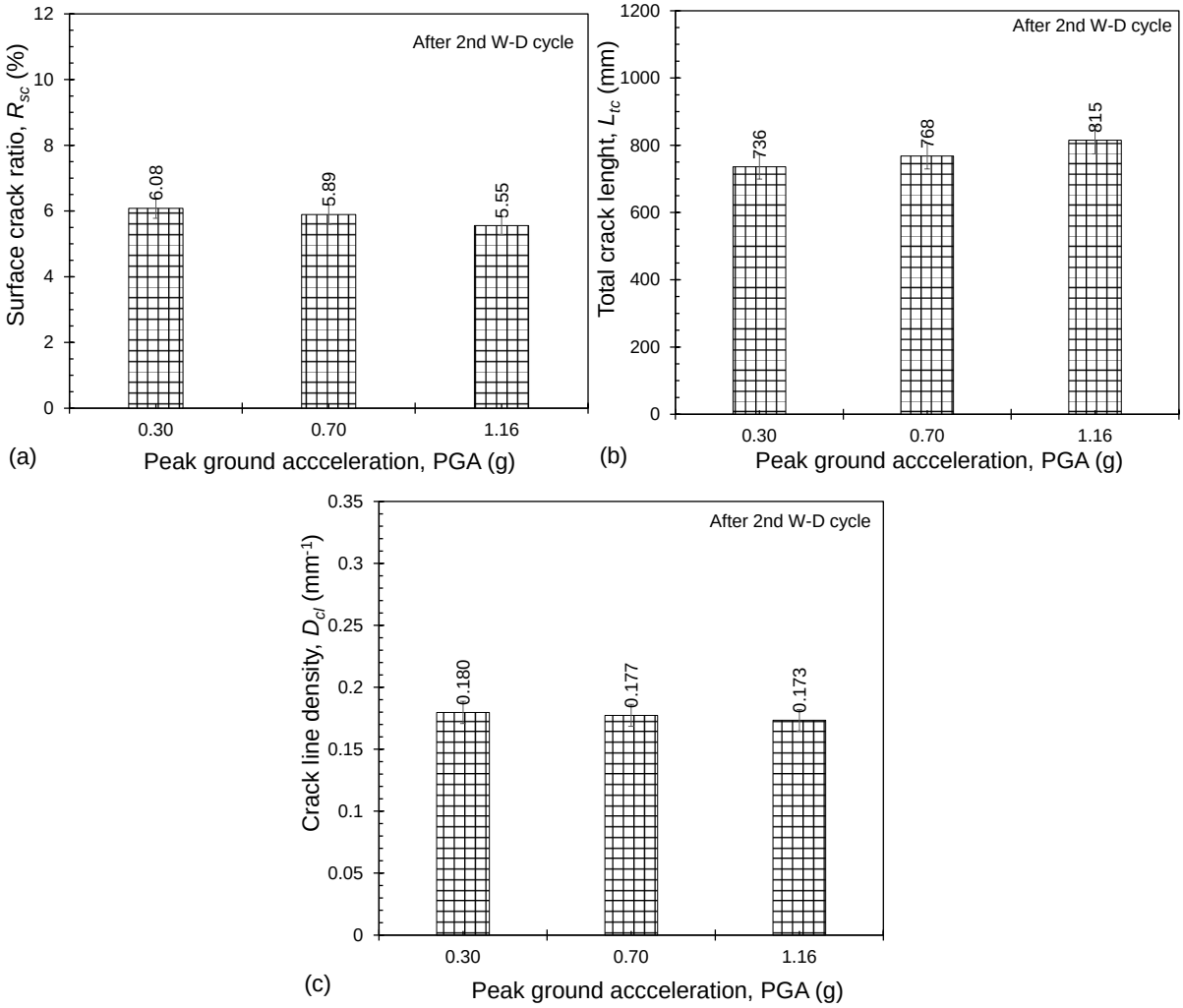

Fig. 8 Effect of VE on (a) R_{sc}; (b) L_{tc}; (c) D_{cl} of untreated samples considering w_0: 18%; γ_{d0}: 14.5 kN/m^3

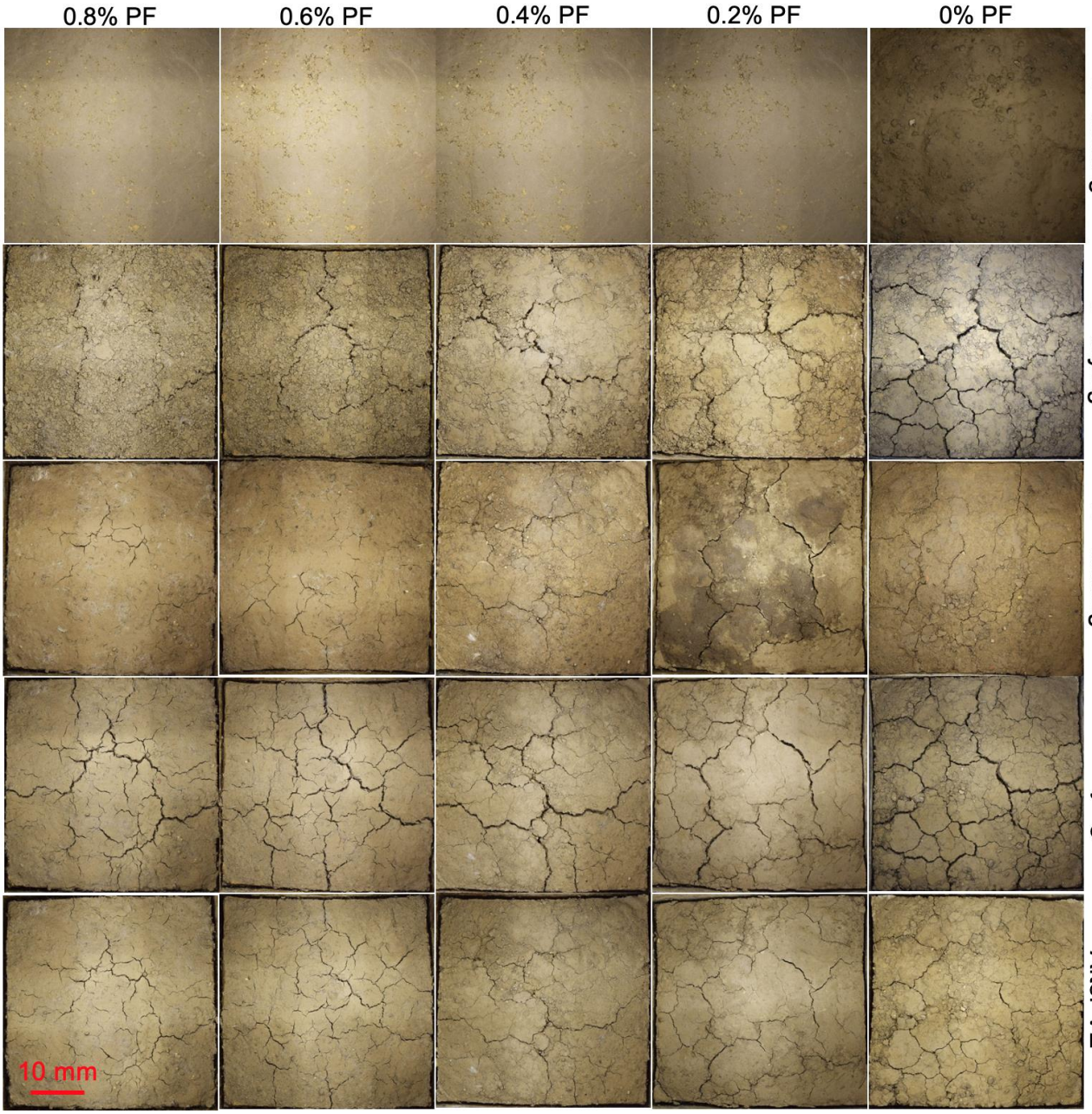

Fig. 9 Effect of W-D cycles and PF on cracks morphology

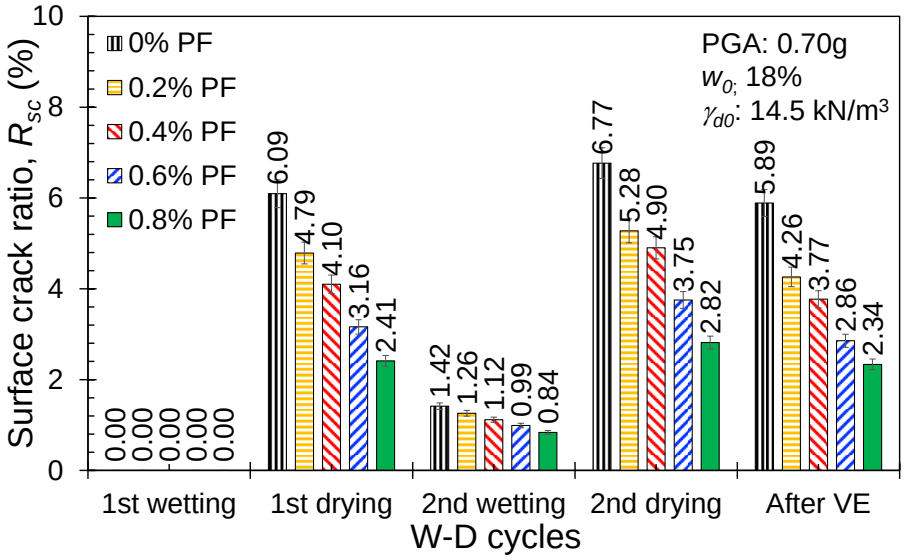

Fig. 10 Effect of W-D cycles and PF on R_{sc}

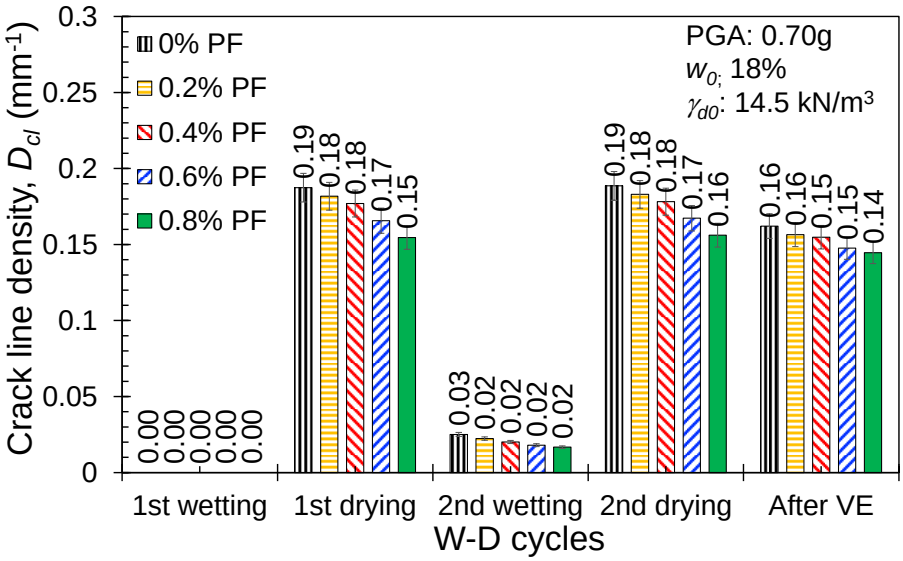

Fig. 11 Effect of W-D cycles and PF on D_{cl}

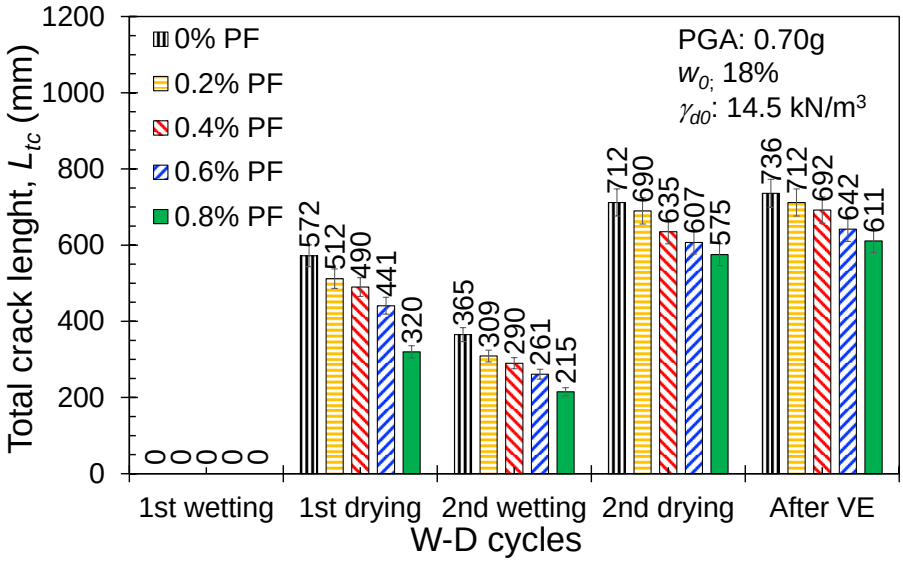

Fig. 12 Effect of W-D cycles and PF on L_{tc}

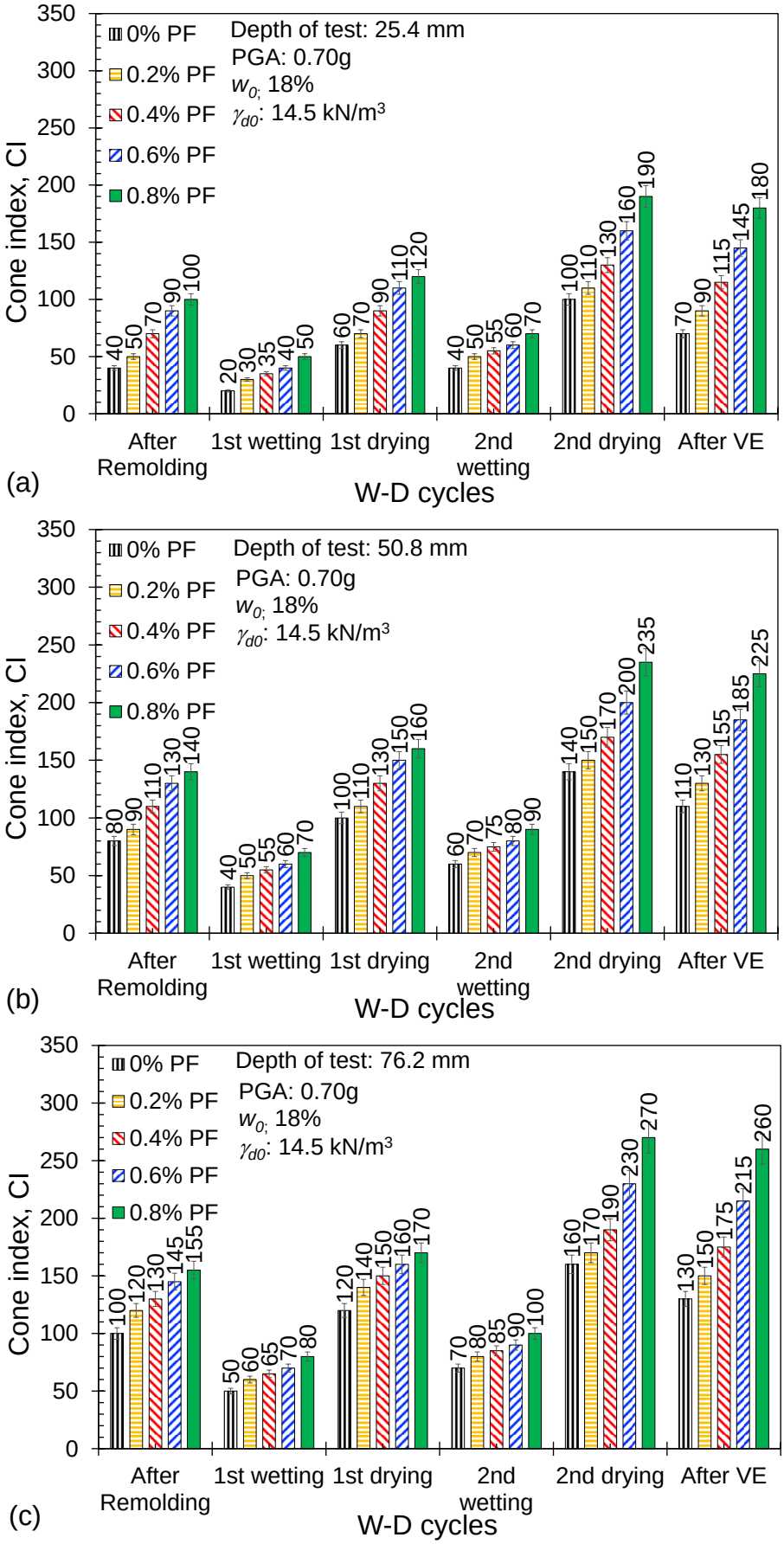

Fig. 13 Effect of W-D cycles and VE on CI at depth of (a) 25.4 mm; (b) 50.8 mm; (c) 76.2 mm

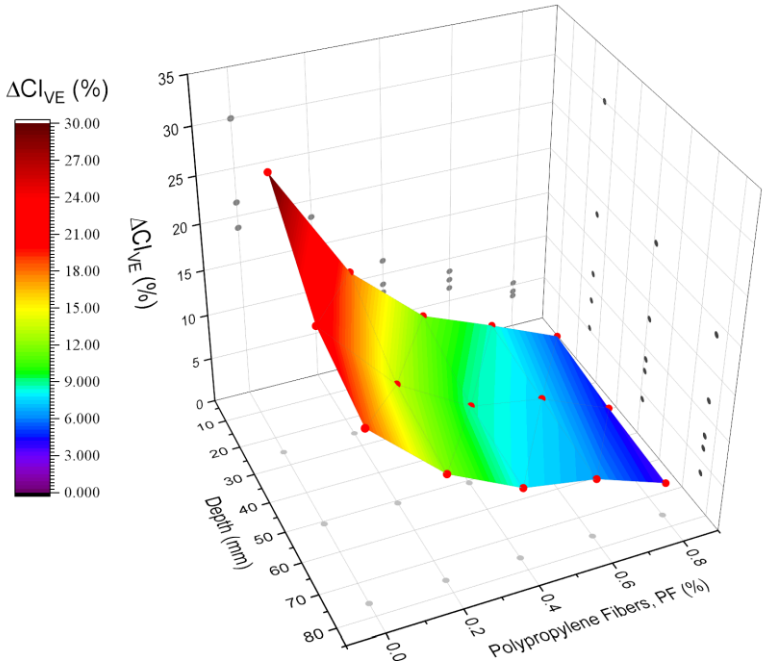

Fig. 14 Effect of W-D cycles and VE on ΔCI_{VE} considering layer depth

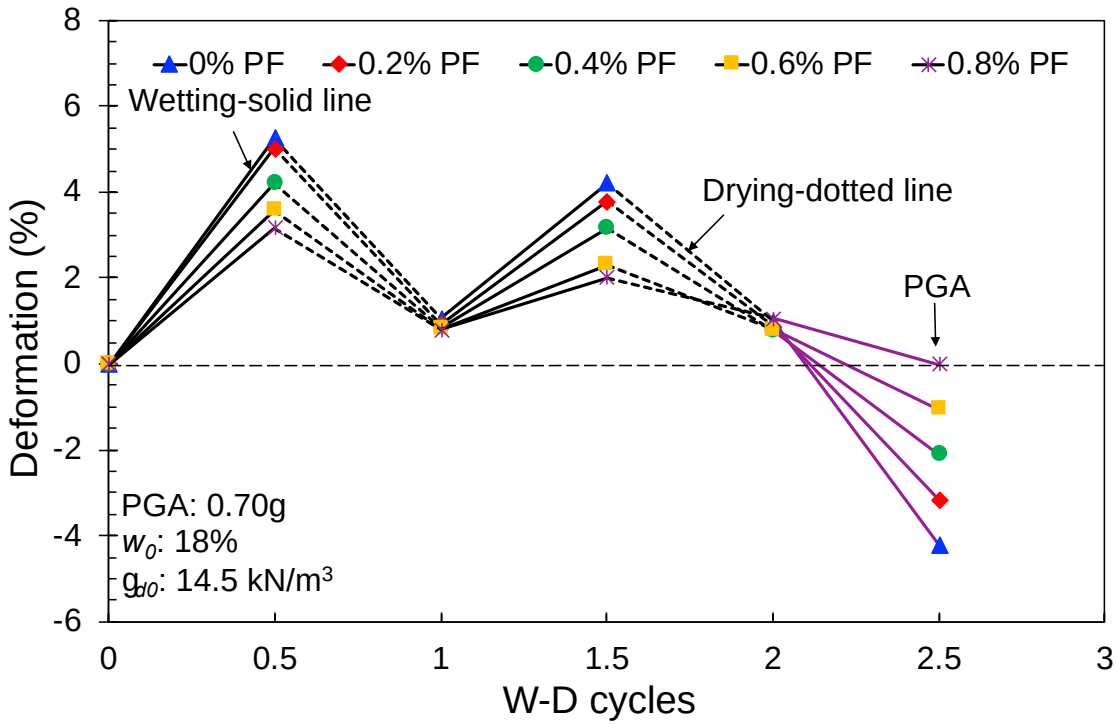

Fig. 15 Effect of W-D cycles and PF on deformation

Table 1 Physical and chemical properties of selected soil

Physical properties	Values	Chemical properties	Values
Clay content (%)	38.10	CaO	1.28
Silt content (%)	56.60	SiO_2	55.88
Sand content (%)	5.30	Al_2O_3	24.524
Liquid limit, w_L (%)	44.50	Fe_2O_3	4.25
Plasticity Index, I_P	20.25	MgO	1.34
Maximum dry unit weight, γ_{dmax} (kN/m^3)	15.85	Na_2O	1.06
Optimum moisture content, w_{opt} (%)	17.60	TiO_2	0.69
Soil classification (USCS)	CL soil	K_2O	1.89

Table 2 Properties of PF

Property	Specification
Chemical Base	100% Polypropylene
Dimensions	Fiber length: 5-6 mm (Blended)
Diameter	10 µm
Density	910 kg/m^3
Tensile Strength	472 MPa
Melting Point	162°C
Ignition Temperature	593°C
Surface	Coated for dispersion
Design	Fine / Fibrillated Fiber
Thermal Conductivity	Low
Electrical Conductivity	Low
Acid Resistance	High
Alkali Resistance	100%

Table 3 Tests matrix of the current study

Analysis	Test/Analysis	Initial water content, w_0 (%)	Initial dry unit weight, γ_{d0} (kN/m^3)	Peak ground acceleration, PGA (g)	Polypropylene fiber, PF (%)	Assessment stages
Desiccation crack analysis	Image analysis	18	14.5	0.70	0, 0.2, 0.4, 0.6, 0.8	After 1st wetting, 1st drying, 2nd wetting, 2nd drying, vibration event
Strength property	Mexe cone penetrometer	18	14.5	0.70	0, 0.2, 0.4, 0.6, 0.8	
Deformation analysis	Vernier Caliber measurements	18	14.5	0.70	0, 0.2, 0.4, 0.6, 0.8	
Preliminary desiccation crack analysis	Image analysis	18	13, 14.5, 16	-	-	After 2nd W-D cycle
		18	14.5	0.30, 0.70, 1.16	-	After vibration event

Table 4 Specifications of shaking table

Description	Specifications
Size of table	4 m x 4 m
Maximum payload	12 ton
Overturning moment	30 ton
Maximum displacement	±250 mm
Maximum velocity	1 m/s
Maximum acceleration	2g